

General Disclaimer

One or more of the Following Statements may affect this Document

- This document has been reproduced from the best copy furnished by the organizational source. It is being released in the interest of making available as much information as possible.
- This document may contain data, which exceeds the sheet parameters. It was furnished in this condition by the organizational source and is the best copy available.
- This document may contain tone-on-tone or color graphs, charts and/or pictures, which have been reproduced in black and white.
- This document is paginated as submitted by the original source.
- Portions of this document are not fully legible due to the historical nature of some of the material. However, it is the best reproduction available from the original submission.



FACILITY FORM 502

N65-40925	
(ACCESSION NUMBER)	(THRU)
25	1
(PAGES)	(CODE)
CR-106452	29
(NASA CR OR TMX OR AD NUMBER)	(CATEGORY)

NGK-16-001-002

Department of Physics and Astronomy
THE UNIVERSITY OF IOWA

Iowa City, Iowa



U. of Iowa 69-38

Alpha Particle Emissivity of the Moon
--An Observed Upper Limit

by

Richard S. Yeh and James A. Van Allen

Department of Physics and Astronomy
University of Iowa
Iowa City, Iowa 52240

July 1969

ABSTRACT

By means of observations with the moon-orbiting spacecraft Explorer 35 during 1967-1968, we find it unlikely that the alpha particle emissivity of the moon is greater than $0.064 \text{ (cm}^2 \text{ sec sr)}^{-1}$ and exceedingly unlikely that it is greater than 0.128, these values being respectively 0.1 and 0.2 of provisional estimates by Kraner et al. in 1966. This result implies that the abundance of ${}_{92}\text{U}^{238}$ in the outer crust (\approx a few meters in thickness) of the moon is very much less than that typical of the earth's lithosphere, though it is consistent with the abundance of ${}_{92}\text{U}^{238}$ in terrestrial basalt or in chondritic meteorites.

INTRODUCTION

On the basis of several physical assumptions of a provisional nature, Kraner et al. (1) suggested in 1966 the possibility of easily detectable quantities of the radioactive noble gases radon ($^{222}_{86}\text{Rn}$) and thoron ($^{220}_{86}\text{Rn}$) in the atmosphere of the moon and on its outermost surface. They estimated the following equivalent surface activities:

Radon: 4 disintegrations ($\text{cm}^2 \text{ sec}$)⁻¹

Thoron: 0.01

The portion of the $^{238}_{92}\text{U}$ radioactive series from $^{222}_{86}\text{Rn}$ to the stable end product $^{206}_{82}\text{Pb}$ yields 4 alpha particles per disintegration ranging in energy from 5.3 to 7.7 MeV. Neglecting thoron and supposing that somewhat less than one-half of the daughter nuclei are lost at each step of the series (by virtue of surface roughness), we adopt

$$\sigma = 8/4\pi = 0.64 (\text{cm}^2 \text{ sec sr})^{-1}$$

as Kraner's provisional estimate of the alpha particle emissivity of the moon.

The effect, if present, is a property of the moon as a total physical system, not of a disembodied sample as measured in the laboratory.

OBSERVING EQUIPMENT

Among other detectors of the University of Iowa equipment on the moon-orbiting spacecraft Explorer 35 of the Goddard Space Flight Center/National Aeronautics and Space Administration is one suitable for a direct determination of the alpha particle emissivity of the moon. The spacecraft was injected into an eccentric lunar orbit on 22 July 1967 and has been operating in an essentially continuous manner since that time. The orbit has been a stable one with mean radial distance to apselene 9386 km and to periselene 2576 km, and orbital period 11.5³ hr (Fig. 1). The plane of the orbit is inclined 168° to the ecliptic.

The pertinent detector (2) is a totally depleted gold-silicon surface barrier one of average thickness 19.6×10^{-4} cm, and frontal area 0.10 cm^2 . The detector is shielded from sunlight by a nickel foil of 0.18 mg cm^{-2} air equivalent thickness for alpha particles and is fitted with a conical collimator of 30° half-vertex angle. Thus, the unidirectional geometric factor of the detector $g = 0.079 \text{ cm}^2 \text{ sr}$. Among the four electronic discrimination levels, the one that is appropriate to the present discussion is designated channel P4. This channel is insensitive to protons and electrons of any energy and detects

with unit efficiency alpha particles in the energy range $2.0 \leq E_{\alpha} \leq 10.2$ MeV, a range well suited to the alpha particles from the radioactive decays noted above. The spacecraft rotates about its axis of maximum moment of inertia with a period of about 2.3 sec. The spin axis of the spacecraft is pointed stably at the south ecliptic pole to within 7° . The axis of the detector is at 90° to the spin axis of the spacecraft. Hence, the detector's field of view sweeps across the moon once per rotation. Pulses from the detector are accumulated in a storage register for a period of 25.57 sec (about ten rotations) each 81.81 sec and the sum is then transmitted.

ANALYSIS OF DATA

Let $\bar{\omega}$ denote the spin-averaged value of the solid angle ω subtended at the detector by that portion of the moon within its field of view at any one instant. The search for lunar-emitted alpha particles exploits the variation of $\bar{\omega}$ as the spacecraft moves in its elliptical orbit. A typical plot of the calculated value of $\bar{\omega}$ vs time is shown in Fig. 2.

The counting rate of channel P4 is the sum of the contributions from three sources:

(1) alpha particles (5.48 MeV) from an $^{241}_{95}\text{Am}$ source that is permanently mounted on the detector to provide an in-flight calibration of the proper operability of the detector and its associated electronics.

(2) solar-emitted alpha particles in interplanetary space and in the earth's magnetospheric tail in the energy range $2.0 \leq E_{\alpha} \leq 10.2$ MeV, and

(3) lunar-emitted alpha particles in the same energy range.

The radius of curvature of the trajectory of an alpha particle moving orthogonal to a magnetic field (the most highly curved case) of typical strength, say, 7×10^{-5} gauss is 30,000 km for $E_{\alpha} = 2$ MeV and 50,000 km for $E_{\alpha} = 6$ MeV. For approximate

purposes it is assumed that both solar and lunar alpha particles travel in straight lines over the distances from the moon that are involved in the present experiment.

Designating the respective contributions to the total counting rate R of detector P4 by the sources (1), (2), and (3) listed above by R_1 , R_2 , and R_3 , one may expect

$$R_1 = a, \text{ independent of } \bar{\omega} \quad (1)$$

$$R_2 = bg (1 - \bar{\omega}/\omega_0) \quad (2)$$

$$R_3 = \sigma g \bar{\omega}/\omega_0 \quad (3)$$

In writing (3), limb brightening has been estimated to be a minor effect and has been neglected. In (1), (2), and (3), a is the rate caused by the calibration source, b is the unidirectional intensity of solar emitted alpha particles in the vicinity of the moon (assumed isotropic, as we find to be usually the case to $\pm 10\%$), ω_0 is the solid angle of the detector = 0.84 sr, and other quantities have been defined previously.

Preliminary examination of early data from Explorer 35 showed σ to be very much less than the estimate of Kraner et al. Subsequent work has been devoted to improving the quantitative sensitivity of the observations.

The principal difficulty, apart from low statistical accuracy, is in selecting periods of time during which interplanetary space is relatively free of solar alpha particles.

We first plotted 3-hr averaged values of the counting rate R of PNH against time for a continuous period of 364 days of observations (decimal day 207/1967 to 205/1968). Tentative blocks of time during which minimal solar alpha particle intensity existed were selected by inspection. Then smaller sub-blocks of time were selected such that no 3-hr averaged counting rate therein departed by more than three standard deviations from the composite mean.

In this way, data were assembled in two separate epochs as follows:

Epoch I: Days 232.1 to 252.9/1967
270.2 to 277.9/1967
285.1 to 291.8/1967
for a total of 35.2 days.

Epoch II: Days 57.9 to 68.7/1968
93.0 to 100.5/1968
138.1 to 143.7/1968
169.8 to 180.1/1968
182.0 to 188.8/1968
for a total of 41.0 days.

During each of the two epochs the observed data were assembled into a unified table of mean counting rate R vs $\bar{\omega}$ in increments $\Delta \bar{\omega} = 0.0125$ sr (cf. Fig. 2). These data were then represented by the weighted least-squares line:

$$R = A + B \bar{\omega}. \quad (4)$$

By relations (1), (2), and (3)

$$R = a + bg (1 - \bar{\omega}/\omega_0) + \sigma g \bar{\omega}/\omega_0. \quad (5)$$

Hence, the observational quantities A and B are related to the physical parameters as follows:

$$A = a + bg, \quad (6)$$

$$B = (\sigma - b) (g/\omega_0), \quad (7)$$

and

$$A + B \omega_0 = a + \sigma g. \quad (8)$$

The quantities $g (= 0.079 \text{ cm}^2 \text{ sr})$ and $g/\omega_0 (= 0.094 \text{ cm}^2)$ are instrumental constants known to an accuracy of a few percent (3).

The best available pre-flight laboratory value of a is $0.0111 \pm 0.0005 \text{ sec}^{-1}$ (3) (4). The flight value of a is clearly less by at least 15%. The precise reason for this is not known. The ${}^{241}\text{Am}$ source was made intentionally a non-thin source in order to smear its alpha particle spectrum and make the consequent

rates of the several channels of the detector somewhat sensitive to effective discrimination levels, etc. Despite considerable effort, the temperature compensation of the complete system was imperfect at the level of several percent over a temperature range of 30° C. Another possible reason for the disparity is inadvertent alpha particle source contamination in the laboratory test chamber. It is therefore clear that the precise value of a must be regarded as unknown. Hence, (6), (7), and (8) provide only two independent relationships among three unknown quantities--the desired quantity σ and the two irrelevant quantities a and b .

Good estimates of a (or at least upper-limits thereof) were obtained by finding the average value of R during several stringently selected days within each of the two epochs such that the intensity of solar protons $0.48 \leq E_p \leq 3.0$ MeV (measured by a different channel of the same detector) divided by the typical p/α ratio as observed during high intensity epochs suggested that b was probably less than $0.006 \text{ (cm}^2 \text{ sec sr)}^{-1}$. An overlapping check of simultaneous data from our similar equipment on earth-orbiting Explorer 33 (far from the moon) gave about the same result. The applicability of the p/α ratio during high intensity epochs to low intensity epochs is a reasonable but unproven physical assumption.

$$\text{Epoch I: } a \leq 0.0093 \pm 0.0003 \text{ sec}^{-1}$$

$$\text{Epoch II: } a \leq 0.0079 \pm 0.0002 \text{ sec}^{-1}$$

Data for Epoch I:

The observed values of R vs $\bar{\omega}$ are shown in Fig. 3.

$$A = 0.0106 \pm 0.0003 \text{ sec}^{-1} \quad (9a)$$

$$B = -0.0086 \pm 0.0035 (\text{sec sr})^{-1} \quad (9b)$$

Using relations (8) and (9) and $a = 0.0093 \pm 0.0003 \text{ sec}^{-1}$

$$\sigma = (A + B \omega_0 - a) / g$$

$$\sigma = -0.0752 \pm 0.0377 (\text{cm}^2 \text{ sec sr})^{-1} \quad (10)$$

Using relations (7) and (9b) and $b = 0.0060 (\text{cm}^2 \text{ sec sr})^{-1}$

$$\sigma = b + B \omega_0 / g$$

$$\sigma = -0.0857 \pm 0.0374 (\text{cm}^2 \text{ sec sr})^{-1} \quad (11)$$

Data from Epoch II:

The observed values of R vs $\bar{\omega}$ are shown in Fig. 4.

$$A = 0.0089 \pm 0.0003 \text{ sec}^{-1} \quad (12a)$$

$$B = -0.0010 \pm 0.0034 (\text{sec sr})^{-1} \quad (12b)$$

Using relations (8) and (12) and $a = 0.0079 \pm 0.0002 \text{ sec}^{-1}$

$$\sigma = +0.0002 \pm 0.0366 (\text{cm}^2 \text{ sec sr})^{-1} . \quad (13)$$

Using relations (7) and (12b) and $b = 0.0060 (\text{cm}^2 \text{ sec sr})^{-1}$

$$\sigma = -0.0047 \pm 0.0363 (\text{cm}^2 \text{ sec sr})^{-1} . \quad (14)$$

DISCUSSION

Physically, σ must be positive or zero.

Using results (10) and/or (11) for Epoch I, the odds against σ being greater than zero are about 14 to 1. This is not an outrageous statistical possibility but does suggest that the adopted value of the solar alpha particle intensity b may have been too small and the corresponding value of a too great. However, no combination of reasonably acceptable values for a and b raises σ above about -0.057 ± 0.036 . Even this result corresponds to odds of 4 to 1 against σ being positive and 600 to 1 against σ being greater than 0.064 (0.1 of Kraner's estimate).

The results (13) and/or (14) are consistent with $\sigma = 0$ and provide odds of 6 to 1 against σ being greater than 0.064 (0.1 of Kraner's estimate) and 1500 to 1 against σ being greater than 0.128 (0.2 of Kraner's estimate).

Thus, we conclude (cf. Figs. 3 and 4) that it is unlikely that σ is greater than 0.1 of Kraner's estimate and exceedingly unlikely that it is greater than 0.2.

REMARKS ON SIGNIFICANCE

It has been remarked by Gold (5) that any gas in the lunar atmosphere, once ionized by solar ultraviolet and/or by charge exchange or collisional ionization by the solar wind, will be immediately swept away by the moving magnetic field in the solar wind (i.e., by the motional electric field). This process may very well be dominant in determining the atmospheric density of stable gases. But for a radioactive gas ($^{86}\text{Rn}^{222}$) of half-life 3.8 days, our estimates for the lifetime against photo-ionization and Michel's estimates (6) for the lifetime against charge exchange and collisional ionization are both too great to be important.

Hence, our result appears to require that the average abundance of $^{92}\text{U}^{238}$ (from which $^{86}\text{Rn}^{222}$ comes) in the outer crust of the moon is less than that in the accessible part of the earth's lithosphere (3 parts per million) (7) by a factor of the order of 10 or greater. It is, however, consistent with the abundance of $^{92}\text{U}^{238}$ in terrestrial basalt or in chondritic meteorites (0.6 ppm and 0.01 ppm, respectively) (8) (9). The thickness of the lunar crust to which these inferences refer is that through which radon can diffuse during its lifetime, i.e., a few meters (10). The result may or may not be applicable to the whole body of the moon.

Work on Explorer 35 data is continuing with some prospect of improving the upper limit on σ reported herein. An apparatus designed specifically for this purpose should have a much larger geometric factor, lower calibration source strength, and several different energy channels.

ACKNOWLEDGEMENTS

The detector on which this work is based was developed and calibrated by Drs. T. P. Armstrong and S. M. Krimigis of this laboratory.

Our work has been supported in part by National Aeronautics and Space Administration grant NGL 16-001-002 and by the U. S. Office of Naval Research contract Nonr 1509(06).

REFERENCES

1. H. W. Kraner, G. L. Schroeder, G. Davidson, and J. W. Carpenter, Radioactivity of the Lunar Surface, Science, 152, 1235-1236, 1966.
2. J. A. Van Allen and N. F. Ness, Particle Shadowing by the Moon, J. Geophys. Res., 74, 71-93, 1969.
3. T. P. Armstrong, private communication.
4. All numerical uncertainties herein are statistical standard deviations.
5. T. Gold, private communication, 1966.
6. F. C. Michel, Interaction between the Solar Wind and the Lunar Atmosphere, Planet. Space Sci., 12, 1075-1091, 1964.
7. J. A. S. Adams, Radioactivity of the Lithosphere, pp. 1-17 of Nuclear Radiation in Geophysics, Academic Press, New York 1962 (H. Israel and A. Krebs, editors).
8. G. J. Wasserburg, G. J. F. MacDonald, F. Hoyle, and W. A. Fowler, Relative Contributions of Uranium, Thorium and Potassium to Heat Production in the Earth, Science, 143, 465-467, 1964.

9. A. P. Vinogradov, Yu. A. Surkov, G. M. Chernov, F. F. Kirnozov, and G. B. Nazarkina, Gamma Investigation of the Moon and Composition of the Lunar Rocks, pp. 77-90 of Moon and Planets. II, North Holland Publishing Co., Amsterdam 1968 (A. Dollfus, editor).
10. G. L. Schroeder, H. W. Kraner, and R. D. Evans, Diffusion of Radon in Several Naturally Occurring Soil Types, J. Geophys. Res., 70, 471-474, 1965.

CAPTIONS FOR FIGURES

Figure 1. A typical orbit about the moon of Explorer 35, as projected on the ecliptic plane. The plane of the orbit is inclined at 168° to that plane (retrograde). X_{SSE} , Y_{SSE} , and Z_{SSE} are selenocentric solar ecliptic coordinates. The numbered tick marks along the orbit designate the time in decimal fractions of the day.

Figure 2. A typical plot of the spin-averaged solid angle $\bar{\omega}$ subtended at the detector by that portion of the moon within its field of view, as the spacecraft moves in its elliptical orbit. This case is referenced to the orbit of Figure 1.

Figure 3. Observed values of the total counting rate R of detector P4 and statistical standard deviations thereof as a function of $\bar{\omega}$ for Epoch I. Data are grouped in increments $\Delta \bar{\omega} = 0.0125$ sr. The arrows on the vertical scale indicate the tentatively adopted value of a ($= 0.0093 \text{ sec}^{-1}$). The principal straight line is the weighted least squares fit to the data. Two auxiliary lines are shown, one the expected dependence of R on $\bar{\omega}$

Figure 3 (cont.)

if $\sigma = 0.64 \text{ (cm}^2 \text{ sec sr)}^{-1}$ (Kraner's estimate) and the other if $\sigma = 0.064$ (0.1 of Kraner's estimate), both taking $a = 0.0093 \text{ sec}^{-1}$ and $b = 0$.

Figure 4. Observed values of the total counting rate R of detector P4 and statistical standard deviations thereof as a function of $\bar{\omega}$ for Epoch II. Data are grouped in increments $\Delta \bar{\omega} = 0.0125 \text{ sr}$. The arrows on the vertical scale indicate the tentatively adopted value of a ($= 0.0079 \text{ sec}^{-1}$). The principal straight line is the weighted least squares fit to the data. Two auxiliary lines are shown, one the expected dependence of R on $\bar{\omega}$ if $\sigma = 0.64 \text{ (cm}^2 \text{ sec sr)}^{-1}$ (Kraner's estimate) and the other if $\sigma = 0.128$ (0.2 of Kraner's estimate), both taking $a = 0.0079 \text{ sec}^{-1}$ and $b = 0$.

DAY 230/1967

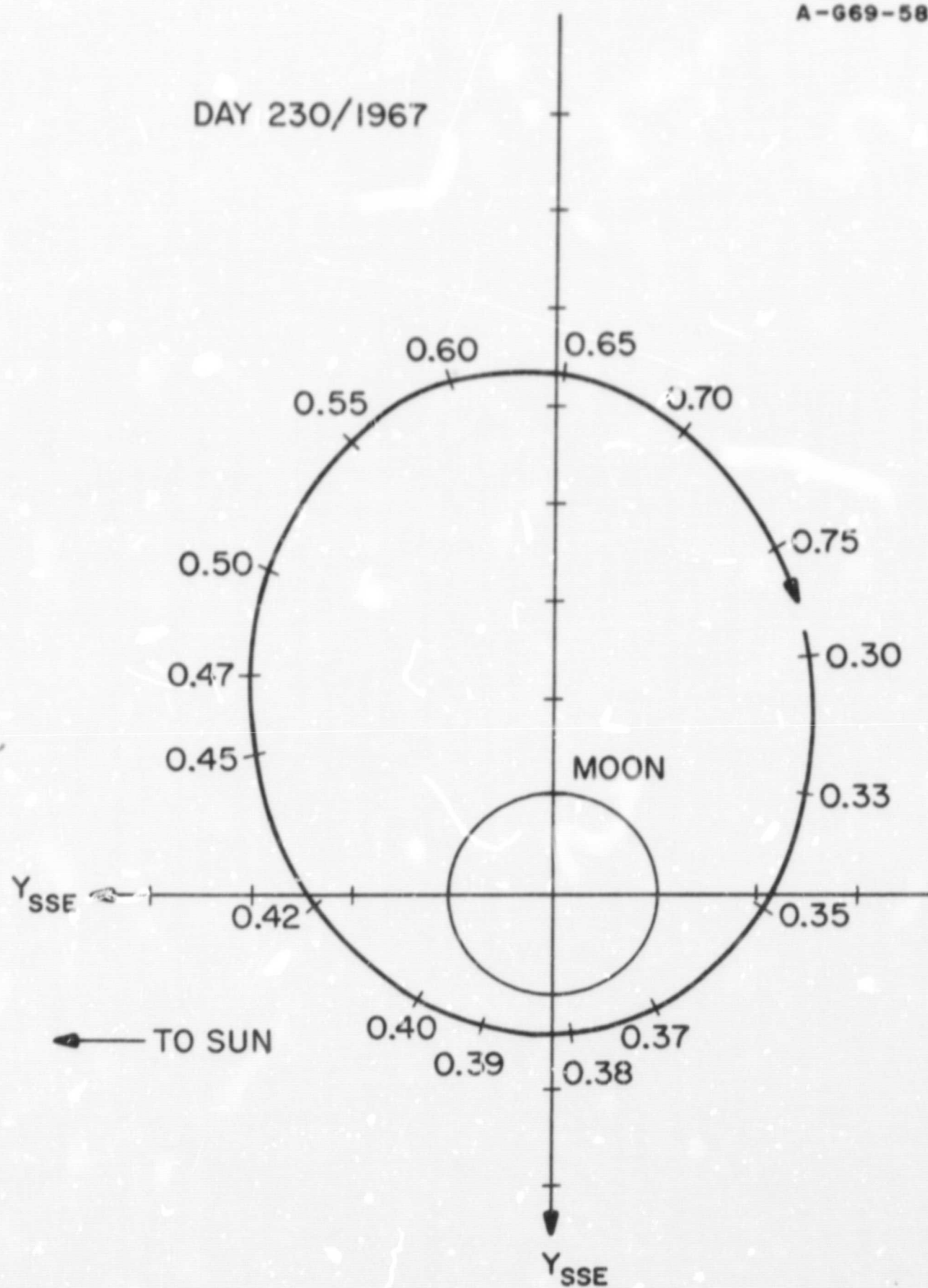


Figure 1

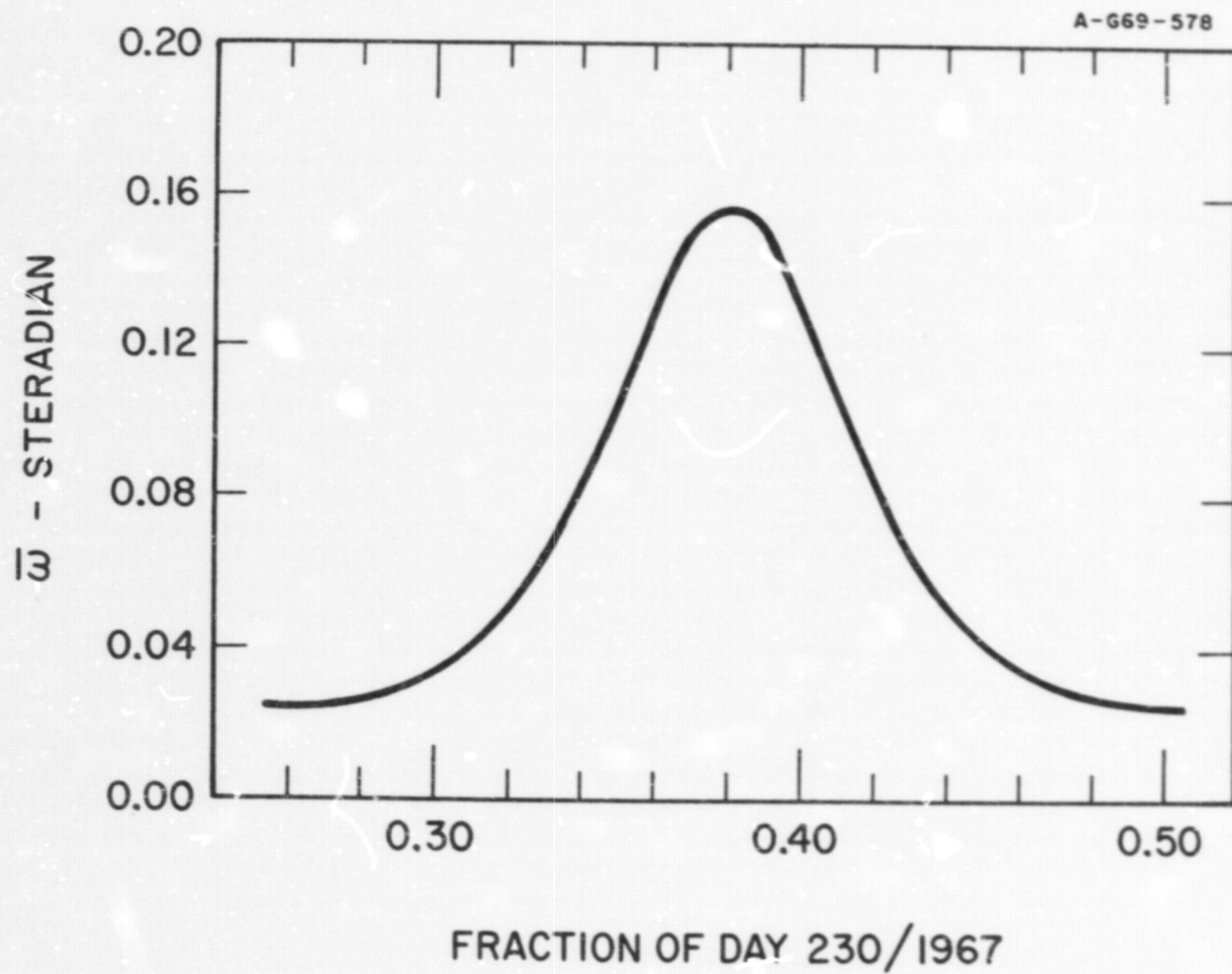


Figure 2

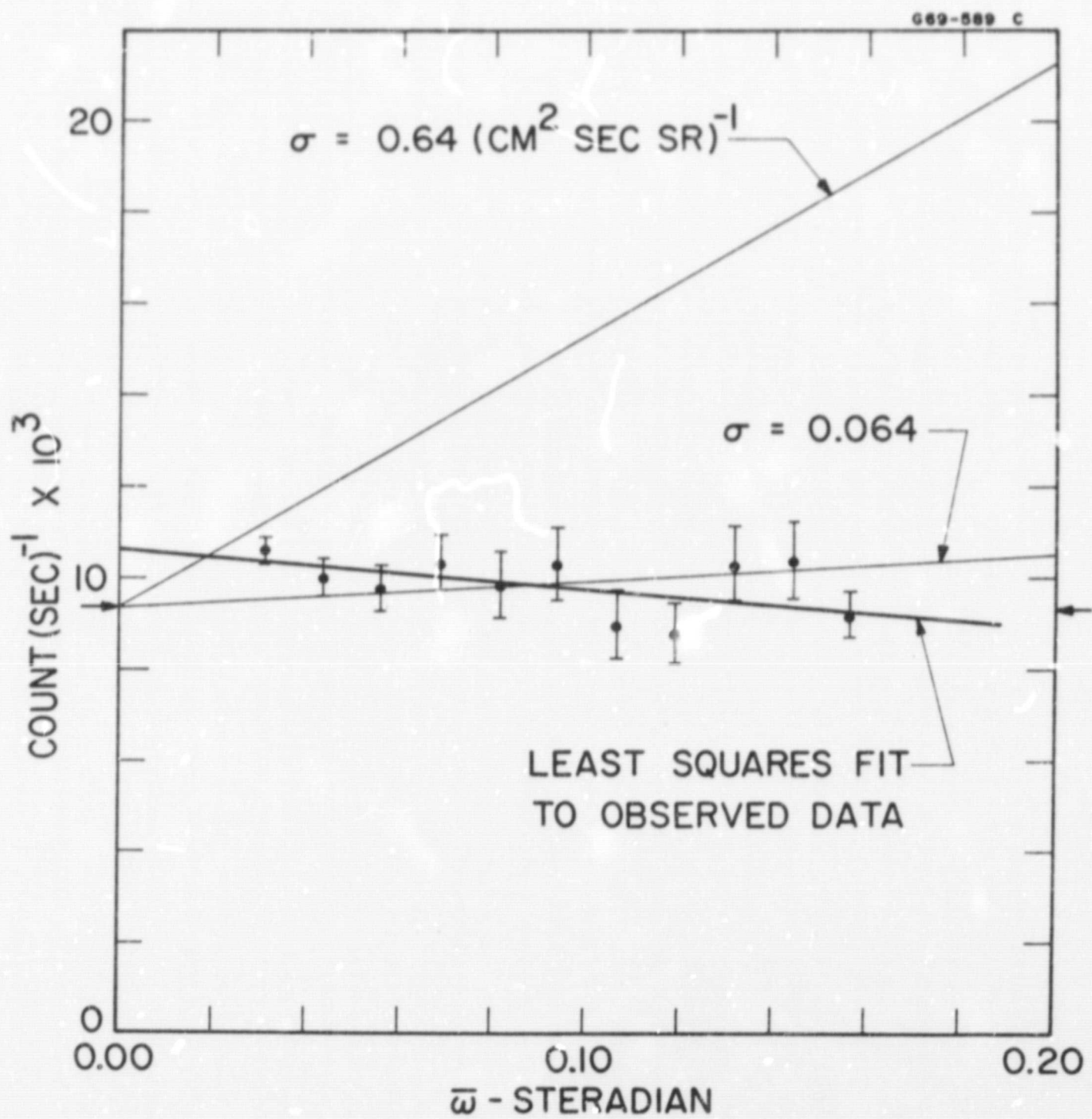


Figure 3

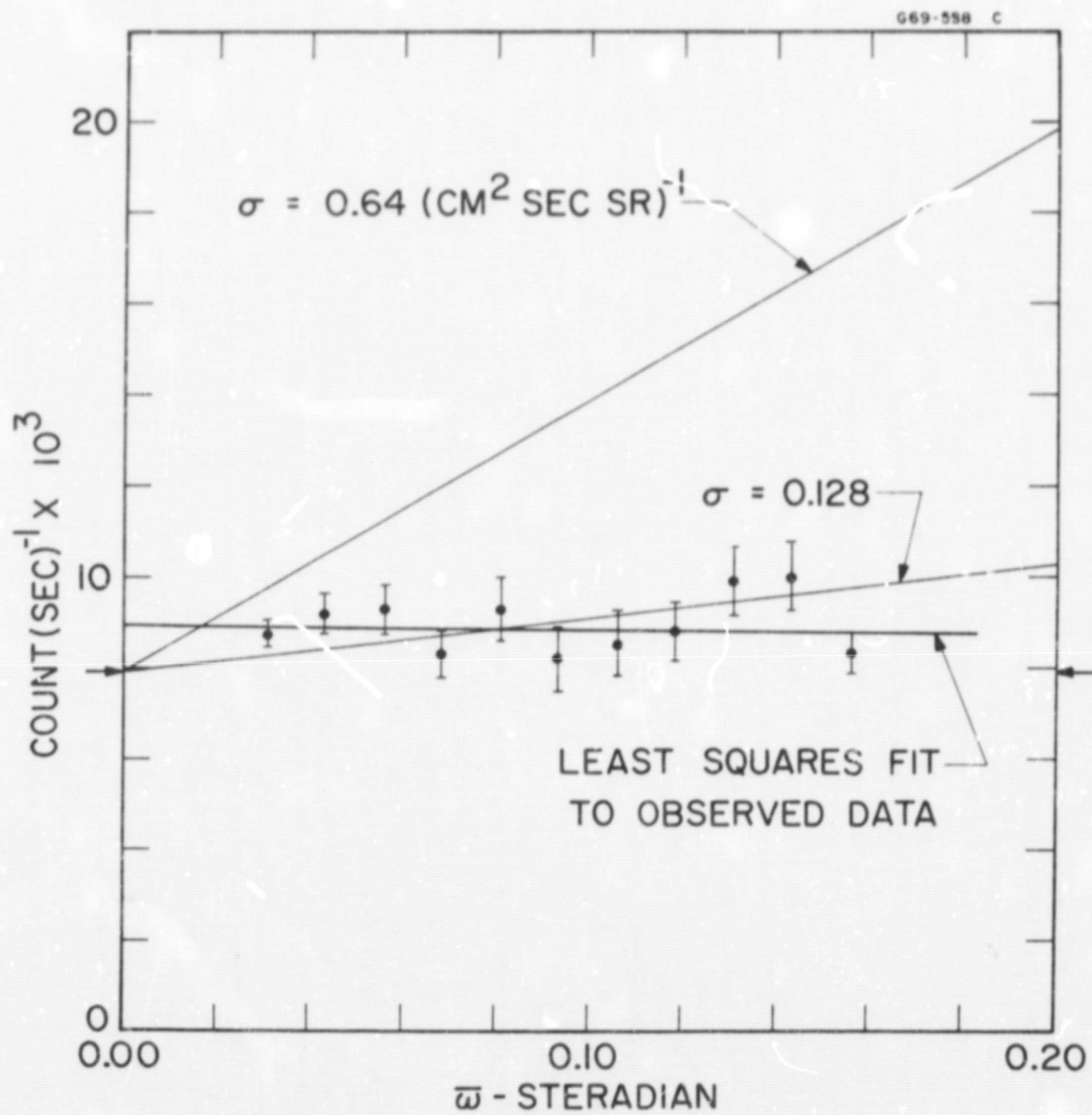


Figure 4